Analytical Methods

PAPER

View Article Online
View Journal | View Issue

CrossMark click for updates

Cite this: *Anal. Methods*, 2015, **7**, 3952

Colorimetric detection of bisphenol A using Au–Fe alloy nanoparticle aggregation†

Xiaosheng Liang,‡ Haibo Wang,‡ Haiying Wang and Guofeng Pei*

A colorimetric assay for bisphenol A (BPA) detection was developed based on Au–Fe alloy nanoparticles. Au–Fe alloy nanoparticles were synthesized and optimized by a hydrothermal method. In the colorimetric assay, horseradish peroxidase was introduced to catalyze BPA polymerization in the presence of hydrogen peroxide, which greatly enhances the sensitivity of the assay. Selectivity is achieved by specific phenol–Fe^{3+} interactions between BPA and the Au–Fe alloy nanoparticles. The limit of detection of BPA is 0.58 μM ($S/D = 3$). The ratio of absorption at 620 nm to absorption at 520 nm is linear with the BPA concentration in the range of 1.10 μM (0.25 mg L^{-1}) to 70.1 μM (16 mg L^{-1}). Parallel spiked and real polycarbonate samples were tested using the proposed method, and the obtained recoveries ranged from 95% to 103% for different samples. This level of detection is on par or slightly better than that achieved by HPLC using UV detection, which is routinely employed to detect BPA. Compared with HPLC, the colorimetric assay for BPA detection exhibits higher throughput and lower cost, making it suitable for the extensive screening of BPA in samples.

Received 13th January 2015
Accepted 30th March 2015

DOI: 10.1039/c5ay00090d

www.rsc.org/methods

Published on 30 March 2015. Downloaded by Duke University on 26/04/2018 22:29:28.

Introduction

Bisphenol A (BPA) is a type of bisphenol that is derived from diphenylmethane. As BPA based plastic is clear and tough, it is employed in the production of many common consumer goods including baby bottles and water bottles as well as for industrial purposes such as water pipe linings. Meanwhile, epoxy resins containing BPA are used as coatings on the inside of many food and beverage cans. In the 1930s, Charles Edward Dodds tested BPA as an artificial estrogen, but he found it to be 37 000 times less effective than estradiol.[1] Recently, the adverse effects of low-dose exposure to BPA have been investigated using animal models. Health issues were identified to result from exposure to BPA during pregnancy and development.[2–5] At present, most countries have banned the use of BPA in baby bottles. However, BPA remains extensively used in industry. Extensive use of BPA results in environmental contamination by this hormone-like compound, which may lead to negative consequences.[6,7] Currently, a number of analytical techniques exist for the detection of BPA. Among them, high performance liquid chromatography (HPLC),[8,9] liquid chromatography coupled with mass spectrometry (LC-MS),[10–12] and enzyme-linked immunosorbent assay (ELISA)[12,13] are the most commonly used techniques. However, these methods are expensive and require dedicated instrumentation. Thus, a new high-throughput and low-cost method that does not require dedicated instruments is urgently needed. Recently, gold nanoparticles (AuNPs) have received considerable attention in the development of visual sensing schemes. The use of AuNPs as a colorimetric reporter relies on their unique surface plasmon resonance (SPR) character. The dispersed or aggregated state of AuNPs corresponds to different SPR states, which are red or blue in color, respectively. Based on this principle, several colorimetric assays have been developed for detection of chemical contamination,[14,15] DNA,[16] proteins,[17] ions,[18,19] amino acids,[20] melamine,[21] viruses,[22] and cancerous cells.[23]

Herein, we demonstrated a colorimetric assay for BPA based on the phenol–Fe^{3+} interactions between BPA and Au–Fe alloy nanoparticles. To increase the sensitivity of this assay, the polymerization of BPA was catalyzed by horseradish peroxidase (HRP), which is able to catalyze the reduction of hydrogen peroxide. In the redox process, a wide range of compounds including aromatic amines and phenols can act as the electron donor;[24,25] consequently, these compounds generate the corresponding free radicals, which are then conjugated or polymerized. These kinds of reactions have been used to synthesize water soluble conducting polymers.[26,27] In this study, HRP catalyzes the polymerization reaction between BPA molecules to form products with numerous phenol groups. These phenol groups interact with Fe^{3+} ions on the surface of Au–Fe alloy nanoparticles, resulting in their aggregation, as shown in Fig. 1.

College of Life Science, South-Central University for Nationalities, Wuhan 430074, People's Republic of China. E-mail: peigf@mail.scuec.edu.cn; Tel: +86 27 6784 2689

† Electronic supplementary information (ESI) available. See DOI: 10.1039/c5ay00090d

‡ These two authors equally contributed to this article.

This journal is © The Royal Society of Chemistry 2015

Published on 30 March 2015. Downloaded by Duke University on 26/04/2018 22:29:28.

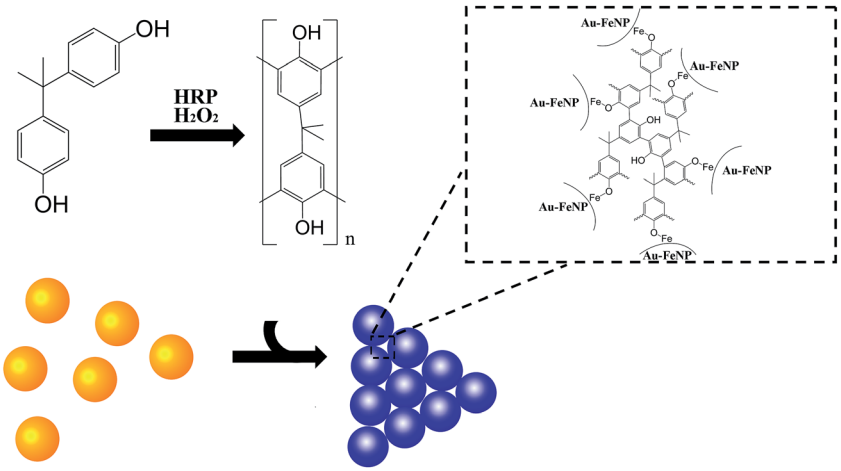

Fig. 1 Scheme of colorimetric detection of bisphenol A using Au–Fe alloy nanoparticles.

Materials and methods

General information

Chloroform, methanol, hydrogen peroxide, hydrogen peroxidase, sodium tetrachloroaurate, ferric chloride, sodium citrate, sodium chloride, and hydrogen chloride were purchased from Sinopharm Chemical Reagent Co, Ltd. (Shanghai, China). Bisphenol A and methanol (HPLC grade) were purchased from J&K Scientific Ltd. (Beijing, China). Agarose was acquired from Invitrogen (Carlsbad, CA, USA). Polycarbonate bottles and polystyrene samples were obtained from a local supermarket. Other reagents and chemicals were at least of analytical grade. Serological plates were obtained from JET Biochemicals Int'l, Inc (Canada). Spectrometric measurements were performed on a synergy HT microplate reader (Bio-Tek Instrument, USA). Transmission electron microscopy (TEM) characterization was carried out on a Tecnai G20 transmission electron microscope (FEI, USA). The infrared spectra were recorded on a Nicolet NEXUS-6700 Fourier transform infrared spectrometer (Thermo Fisher Scientific, USA).

Preparation of Fe–Au alloy nanoparticles

Fe–Au alloy nanoparticles were prepared by a previously reported trisodium citrate reduction method with modifications.[28] Briefly, trisodium citrate (10 mL, 38.8 mM) was rapidly added to a boiling solution of $HAuCl_4$ and $FeCl_3$ (100 mL, 1 mM in total), and the solution was continually boiled for another 30 min to yield a wine-red solution. After filtering the solution through a 0.22 μm Millipore syringe filter to remove the precipitate, the filtrate was stored in a refrigerator at 4 °C.

Characterization of Fe–Au alloy nanoparticles

Agarose gel electrophoresis analysis. Agarose gel electrophoresis analysis was carried out in accordance with the previously reported method.[29] Fe–Au alloy nanoparticles or AuNPs (20 μL) mixed with 50% glycerol (5 μL) were loaded into a 0.8% agarose gel with running buffer (20 mM Tris–acetate, pH 7.0). Electrophoresis was run for 20 min at 100 V. The gel was imaged by using a digital camera.

TEM imaging. Grids previously coated with evaporated carbon were floated on drops of samples on Parafilm for 10 min. Excess solution was removed from the grid by carefully touching the edge of the grid onto the filter paper. The samples were not negatively stained. The grids were allowed to dry overnight. TEM images were captured with a transmission electron microscope (Tecnai G20, FEI) system. High resolution TEM images were captured with a field emission high resolution transmission electron microscope (JEM 2100F STEM/EDS, JEOL) system.

Fourier transform infrared (FTIR) spectroscopy. BPA or the dried polycarbonate extract was mixed with spectrally pure KBr and ground to a powder. Subsequently, a potassium bromide disk was prepared for FTIR detection.

Sample pretreatment

The pretreatment procedure was similar to that reported for chromatography. Briefly, polycarbonate bottles and polystyrene samples were cut into 0.2 g pieces, which were then dissolved in 10 mL chloroform by 20 min of sonication at a frequency of 20 kHz and a power of 277 W (Sonics VC 750, Vibra-Cell, France). Methanol was added to the resulting solution to precipitate macromolecular compounds. After centrifuging the sample at 8000*g* for 10 min, the supernatant was filtered through a 0.22 μm membrane. The supernatant was then evaporated to dryness, and the residue was dissolved in 2 mL of hot water.

Colorimetric assays

To measure BPA in the samples, 40 μL of the BPA containing sample after pretreatment and 200 μL of the Au–Fe alloy nanoparticles were pipetted into the wells of a serological plate and then mixed together. Subsequently, 5 μL of HRP solution (3 μM; the extinction coefficient of HRP at 403 nm is 9.921×10^4 L mol^{-1} cm^{-1} (ref. 30)) and 5 μL of hydrogen

Published on 30 March 2015. Downloaded by Duke University on 26/04/2018 22:29:28.

peroxide (0.3% w/v) were added into the wells. After a few minutes of incubation, the colour changes were observed either by the naked eye or from the absorbance values of the solutions measured using the microplate reader (synergy HT Biotek).

Results and discussion

Optimization of the synthesis of Au–Fe alloy nanoparticles

Different ratios of Au and Fe^{3+} were adopted to synthesize Au–Fe alloy nanoparticles. Under 1 mM ferric and gold ion concentration in total ferric ions increased from 1 μM to 0.5 mM, red wine-colored Au–Fe alloy nanoparticle colloidal solutions were prepared. To optimize the ratio of Au^{3+} to Fe^{3+} in the precursors, different concentrations of Au^{3+} and Fe^{3+} were used to synthesize Au–Fe alloy nanoparticles. Subsequently, the absorptions of the resultant nanoparticles at 520 and 620 nm were measured in the presence of polymerized BPA. The ratio of the absorption readings at 620 nm to those at 520 nm indicated whether the nanoparticles were in the aggregated or dispersed state. In this study, the nanoparticles with the greatest absorption ratio exhibited the best phenol binding ability. The results indicated that as the concentration of Fe ions increased from 1 μM to 0.1 mM, the Au–Fe alloy nanoparticles exhibited more significant aggregation in the presence of polymerized BPA. As the Fe ion concentration increased further from 0.1 mM to 0.5 mM, fewer Au–Fe alloy nanoparticle aggregates formed. Among the samples, the Au–Fe alloy nanoparticles synthesized using 0.1 mM Fe^{3+} as a precursor exhibited the greatest amount of aggregation (Fig. S1†). Further experiments investigated Au–Fe alloy nanoparticles synthesized using 0.1 mM Fe^{3+} as a precursor. XPS characterization was conducted to verify the introduction of Fe^{3+} to the nanoparticle surface (Fig. S2†). After repeated washing and centrifugation, the XPS spectra of the vacuum-dried nanoparticles were obtained. The peaks of Au, O, and C were found in both spectra. The Fe 2p peak was observed in the spectrum of the Au–Fe alloy nanoparticles, indicating that Fe^{3+} ions exist on the nanoparticle surfaces after repeated washings.

Nanoparticle characterization

Au–Fe alloy nanoparticles were characterized by UV-Vis spectroscopy, gel electrophoresis, and TEM, as shown in Fig. 2. The UV-Vis spectra showed that the absorption of Au–Fe alloy nanoparticles at 520 nm was significantly increased compared with the absorption of gold nanoparticles. The addition of BPA to the Au–Fe alloy nanoparticles decreased the absorption near 520 nm and caused a red-shift of 3 nm. Polymerized BPA greatly decreased the absorption of the Au–Fe alloy nanoparticles near 520 nm resulting in further red shifting; the maximum absorption peak of Au–Fe alloy nanoparticles was red shifted by 30 nm upon the addition of polymerized BPA. The red shifting of the nanoparticle UV-Vis absorption peak due to BPA or polymerized BPA indicates that BPA or polymerized BPA interacted with the Au–Fe alloy nanoparticles. As reported previously,[31,32] this interaction is based on the bonding between the phenol hydroxyl groups of BPA or polymerized BPA with Fe^{3+} ions on the nanoparticle surfaces. The electrophoresis results show that the Au–Fe alloy nanoparticles traveled slower than the AuNPs due to the introduction of Fe^{3+}, which changes the surface electric charges. Furthermore, crystal growth is influenced as well, resulting in a change in the nanoparticle size (Fig. S3†). The electrophoresis results also show that the Au–Fe alloy nanoparticles traveled slower than the Au–Fe alloy nanoparticles with BPA (Fig. 2); again indicating that BPA interacted with the Au–Fe alloy nanoparticles. The phenol–Fe^{3+} interaction between BPA and the Au–Fe alloy nanoparticles reduced the positive charge on the nanoparticle surface and increased the hydrated radius of the

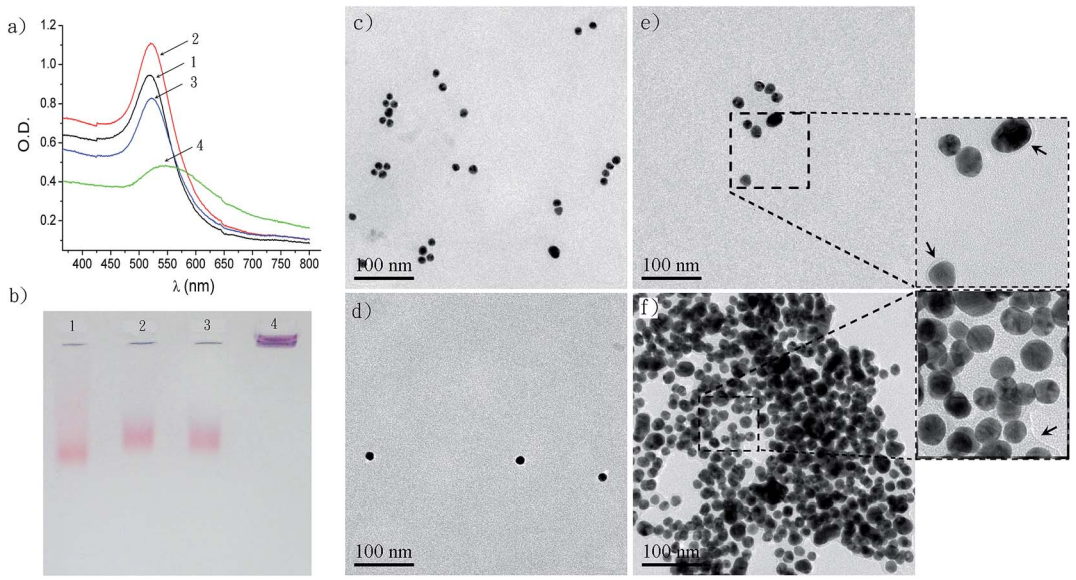

Fig. 2 (a) UV-Vis spectra and (b) agarose gel electrophoresis analysis of the following: (1) 13 nm AuNPs; (2) Au–Fe alloy nanoparticles; (3) Au–Fe alloy nanoparticles with 200 μM BPA; and (4) Au–Fe alloy nanoparticles with HRP-catalyzed polymerized BPA. (c–f) The TEM images of the above samples 1–4, respectively.

 This journal is © The Royal Society of Chemistry 2015

Published on 30 March 2015. Downloaded by Duke University on 26/04/2018 22:29:28.

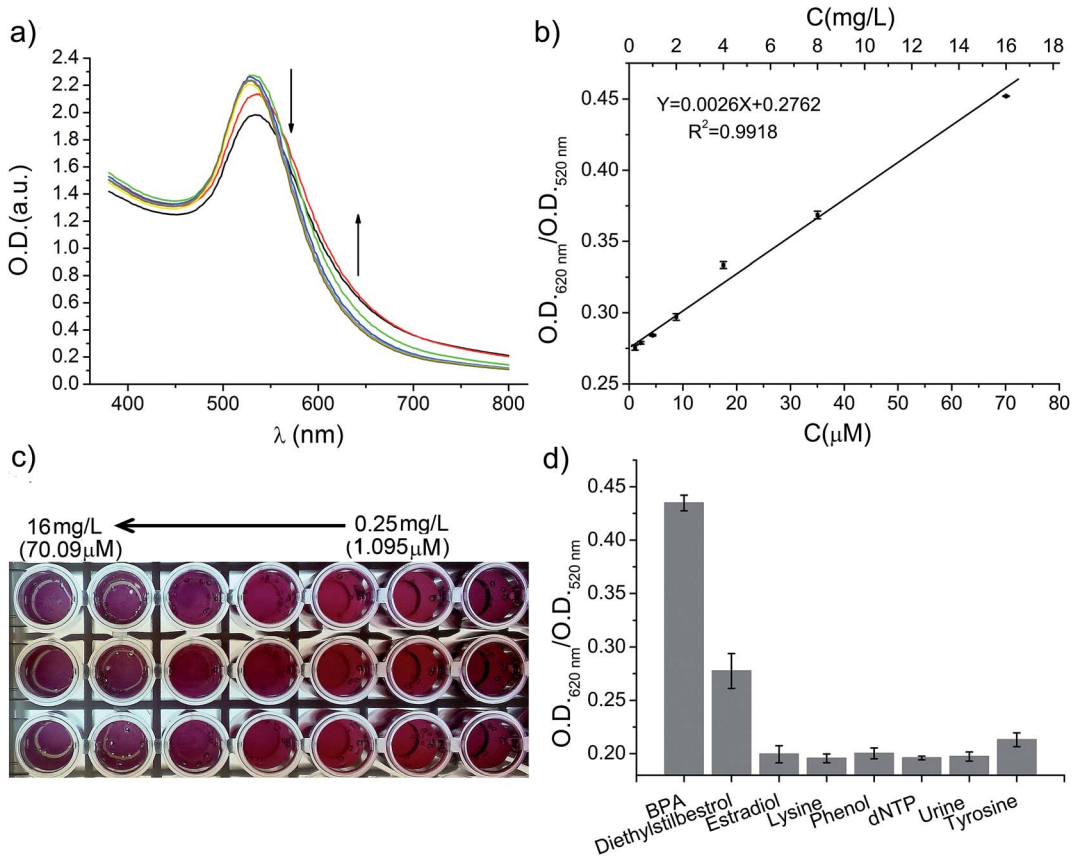

Fig. 3 Colorimetric assay of BPA: (a) the UV-Vis spectra of the Au–Fe alloy nanoparticles, HRP, and the hydrogen peroxide mixture with different BPA concentrations. (■) BPA 16 mg L^{-1}, (■) BPA 8 mg L^{-1}, (■) BPA 4 mg L^{-1}, (■) BPA 2 mg L^{-1}, (■) BPA 1 mg L^{-1}, (■) BPA 0.5 mg L^{-1}, (■) BPA 0.25 mg L^{-1}, and (■) BPA 0 mg L^{-1}. (b) The calibration curves of BPA. (c) Visual colour changes of Au–Fe alloy nanoparticles under different BPA concentrations. (d) The ratio of absorbance readings at 620 nm to those at 520 nm in the presence of BPA, diethylstilbestrol, estradiol, lysine, phenol, DNTP, urea and tyrosine (from left to right). Concentration: 15 μM each.

nanoparticles, resulting in slower electrophoretic migration. The electrophoresis lane containing the Au–Fe alloy nanoparticles and the polymerized BPA mixture remained in the sampling hole; this may have resulted from the aggregation of Au–Fe alloy nanoparticles due to the interactions of the phenol groups of polymerized BPA with the Fe^{3+} ions of the nanoparticles.

The HRTEM image of Au–Fe alloy nanoparticles (Fig. S4†) showed that iron oxide nanostructures formed around AuNPs. And, no core–shell structure was observed. The TEM images show that the Au–Fe alloy nanoparticles in the presence of 200 μM BPA exhibited a low electron density "shell" (Fig. 2e). Compared to the samples of Fig. 2d and S4,† BPA is the only extra additive in the sample of Fig. 2e. The shell like structure should be constituted by BPA. The forming of the shell like structure provides additional evidence for the interaction between BPA and the Au–Fe alloy nanoparticles. The presence of HRP-catalyzed BPA polymers resulted in the aggregation of Au–Fe alloy nanoparticles (Fig. 2f); the TEM images show membrane like structures around aggregated nanoparticles, demonstrating the polymerization of BPA under HRP catalysis. Meanwhile, no obvious aggregation was observed in the TEM images of Au–Fe alloy nanoparticles in the presence of HRP and hydrogen peroxide (Fig. S5†). This verifies that BPA is the only factor causing Au–Fe alloy nanoparticles aggregation under the current experimental conditions.

Detection calibration ranges and sensitivity

A BPA solution was sequentially diluted to generate samples for colorimetric assays. Fig. 3a shows the absorption spectra of the

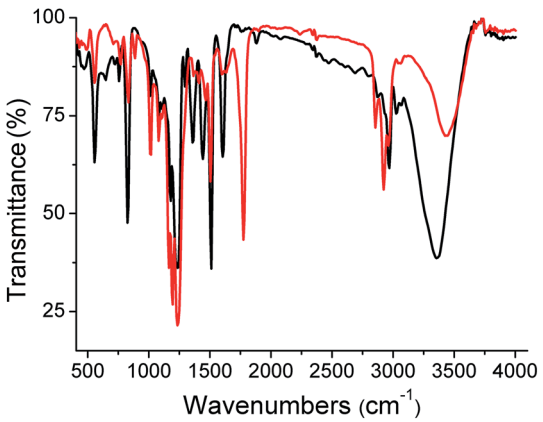

Fig. 4 Infrared spectra of BPA (black curve) and polycarbonate extract (red curve).

Table 1 Results of the determination of real BPA samples

	μM per ppm			
Samples[a]	Original[b]	Spiked	Found	Recovery%
Spiked polystyrene		219.0/50	209.0 ± 4.3/47.7 ± 1.0	95.4 ± 2.1
		547.5/125	565.5 ± 19.2/129.1 ± 4.4	103.3 ± 3.4
		1095/250	1129.7 ± 11.3/257.9 ± 2.6	103.2 ± 1.0
Polycarbonate bottle	161.2 ± 6.6/36.8 ± 1.5		157.8 ± 3.0/36.0 ± 0.7	97.9 ± 1.9
	112.7 ± 2.8/25.7 ± 0.6		108.8 ± 1.4/24.8 ± 0.3	96.5 ± 1.3
	222.7 ± 6.4/50.8 ± 1.5		230.1 ± 4.1/52.5 ± 0.9	103.3 ± 1.8

[a] Average of three repeated measurements. [b] Detected by HPLC.

Published on 30 March 2015. Downloaded by Duke University on 26/04/2018 22:29:28.

Au–Fe alloy nanoparticles, HRP, and hydrogen peroxide mixture with different BPA concentrations. The spectra show that as the BPA concentration increased, the absorption at 520 nm decreased, while the absorption around 620 nm increased. The BPA response was evaluated by the ratio of absorption readings at 620 nm to those at 520 nm. In Fig. 3b, the responses of BPA could be calibrated from 1.10 μM (0.25 mg L^{-1}) to 70.1 μM (16 mg L^{-1}). A detection limit of 0.58 μM (132.0 μg L^{-1}) was acquired ($S/N = 3$). The calibration range achieved in this study is similar to the one of the HPLC method with UV detection, and the detection limit of our method is small enough for BPA detection in polycarbonate samples.

Selectivity

We chose some interferents that may exist in biological or environmental samples to study the specificity of this sensor. Diethylstilbestrol, estradiol, lysine, phenol, dNTP, urea and tyrosine were chosen as representatives of estrogens, amino acids, structural analogues and metabolites. Fig. 3d shows that a dramatic red-shift of the Au–Fe alloy nanoparticles could be observed for BPA in the concentration of 15 μM, but not for estradiol, lysine, phenol, dNTP, urea or tyrosine. Diethylstilbestrol could induce obvious colour change. These results indicate that other molecules with the bisphenol or polyphenol structure could interfere with the BPA detection; nevertheless, estrogen in nature is much less than the concentration we tested. Tyrosine and phenol have a functional group of phenol. Theoretically, phenol could polymerize as well. In this research, tiny Au–Fe alloy nanoparticle aggregation was detected for tyrosine, but not for phenol. The main reason for this is denaturation of HRP caused by phenol. These results suggest that this method has excellent selectivity for BPA.

Spiked and real sample detection

Because polystyrene has a similar solubility to BPA in organic solvents, BPA was spiked into polystyrene samples to evaluate the new nanoparticle aggregation method for the detection of BPA in samples. To validate the proposed method for BPA in real samples, amounts of BPA in polycarbonate drink bottles were measured by the Au–Fe alloy nanoparticle aggregation assay after sample pretreatment. The IR spectra of the dried polycarbonate extract and the BPA standard sample were then collected; the spectra show that the dried polycarbonate extract exhibited a similar absorption to the BPA standard sample, as shown in Fig. 4. The peaks at 825 cm^{-1} and 1511 cm^{-1} are coinciding with the absorption of the benzene skeleton and the vibration of *para*-substituted groups, respectively. The peak at 3340 cm^{-1} corresponds to the absorption of phenol groups. According to these results, our pretreatment procedure resulted in BPA being contained in the polycarbonate extract.

Parallel detection of the same samples was performed by HPLC to define the BPA concentration in the real sample extracts (Fig. S6†). The HPLC results of the spiked polystyrene samples and real polycarbonate sample are summarized in Table 1. As shown in Table 1, excellent recoveries in the range of 95 to 103% were obtained for all samples, suggesting that the proposed method is reliable and suitable for real applications. In this research, we have developed an efficient Au–Fe alloy nanoparticle aggregate system for BPA detection in real samples. The Au–Fe alloy nanoparticles act as signal convertors that translate the BPA–nanoparticle interaction into changes in SPR signals. Meanwhile, the Fe introduced into the nanoparticles interacts with the phenol groups of BPA to serve as a detector. In this system, the catalysis of BPA polymerization by HRP increases the detection sensitivity. The proposed method displays a high sensitivity and a low limit of detection for the determination of BPA and can be applied to the determination of BPA in real samples with satisfactory recoveries. Such an alloyed nanoparticle aggregation system may open a new pathway for the design of biosensors.

Conclusions

In summary, based on phenol–Fe^{3+} interactions between BPA and Au–Fe alloy nanoparticles and HRP catalyzed BPA polymerization in the presence of hydrogen peroxide, we presented a new scheme for sensitive, low cost and onsite detection of BPA in real samples. Applying this method the limit of detection for BPA is 0.58 μM. The range of quantification is from 1.10 μM (0.25 mg L^{-1}) to 70.1 μM (16 mg L^{-1}), which fulfils the need for screening of BPA in material or environmental samples.

Acknowledgements

This work was funded by the National Natural Science Foundation of China (grant no. 31300829), the Natural Science

 This journal is © The Royal Society of Chemistry 2015

Published on 30 March 2015. Downloaded by Duke University on 26/04/2018 22:29:28.

Foundation of Hubei Province of China (grant no. 2014CFC1117), the Special Fund for Basic Scientific Research of Central Colleges, the South-Central University for Nationalities (grant no. CZQ11031) and the Special Fund for Quality Supervision Research in the Public Interest (grant no. 201310141). The authors would like to thank Enago (http://www.enago.cn) for the English language review.

Notes and references

1 E. Dodds and W. Lawson, *Nature*, 1936, **137**, 996.
2 S. M. Ho, W. Y. Tang, J. Belmonte de Frausto and G. S. Prins, *Cancer Res.*, 2006, **66**, 5624–5632.
3 C. M. Markey, P. R. Wadia, B. S. Rubin, C. Sonnenschein and A. M. Soto, *Biol. Reprod.*, 2005, **72**, 1344–1351.
4 M. Munoz-de-Toro, C. M. Markey, P. R. Wadia, E. H. Luque, B. S. Rubin, C. Sonnenschein and A. M. Soto, *Endocrinology*, 2005, **146**, 4138–4147.
5 T. J. Murray, M. V. Maffini, A. A. Ucci, C. Sonnenschein and A. M. Soto, *Reprod. Toxicol.*, 2007, **23**, 383–390.
6 C. M. Ignatius, E. E. Francis, E. N. Emeka, N. S. Elvis and J. I. Ebele, *Bull. Environ. Contam. Toxicol.*, 2010, **85**, 534–537.
7 W. Zhao, N. Sheng, R. Zhu, F. Wei, Z. Cai, M. Zhai, S. Du and Q. Hu, *J. Hazard. Mater.*, 2010, **179**, 223–229.
8 Y. Watabe, T. Kondo, H. Imai, M. Morita, N. Tanaka, J. Haginaka and K. Hosoya, *Anal. Sci.*, 2004, **20**, 133–137.
9 C. H. Wu, D. S. Ren, Y. H. He, L. X. Zheng and Z. J. Zhou, *Chin. J. Ind. Hyg. Occup. Dis.*, 2011, **29**, 856–858.
10 D. Battal, I. Cok, I. Unlusayin and B. Tunctan, *Biomed. Chromatogr.*, 2014, **28**, 686–693.
11 J. Sajiki, Y. Hasegawa, H. Hashimoto, Y. Makabe, F. Miyamoto, R. Yanagibori, J. Shin, Y. Shimidzu and T. Morigami, *Toxicol. Mech. Methods*, 2008, **18**, 733–738.
12 S. M. Zimmers, E. P. Browne, P. W. O'Keefe, D. L. Anderton, L. Kramer, D. A. Reckhow and K. F. Arcaro, *Chemosphere*, 2014, **104**, 237–243.
13 Y. Lu, J. R. Peterson, J. J. Gooding and N. A. Lee, *Anal. Bioanal. Chem.*, 2012, **403**, 1607–1618.
14 Z. Y. Zhang, Z. P. Chen, S. S. Wang, C. L. Qu and L. X. Chen, *ACS Appl. Mater. Interfaces*, 2014, **6**, 6300–6307.
15 L. Chen, W. H. Lu, X. K. Wang and L. X. Chen, *Sens. Actuators, B*, 2013, **182**, 482–488.
16 X. Bai, C. Shao, X. Han, Y. Li, Y. Guan and Z. Deng, *Biosens. Bioelectron.*, 2010, **25**, 1984–1988.
17 L. J. Ou, P. Y. Jin, X. Chu, J. H. Jiang and R. Q. Yu, *Anal. Chem.*, 2010, **82**, 6015–6024.
18 Y. Guo, Z. Wang, W. Qu, H. Shao and X. Jiang, *Biosens. Bioelectron.*, 2011, **26**, 4064–4069.
19 L. Chen, J. H. Li and L. X. Chen, *ACS Appl. Mater. Interfaces*, 2014, **6**, 15897–15904.
20 W. Pu, H. Zhao, C. Huang, L. Wu and D. Xu, *Anal. Chim. Acta*, 2013, **764**, 78–83.
21 X. Liang, H. Wei, Z. Cui, J. Deng, Z. Zhang, X. You and X. E. Zhang, *Analyst*, 2011, **136**, 179–183.
22 Y. Seetang-Nun, W. Jaroenram, S. Sriurairatana, R. Suebsing and W. Kiatpathomchai, *Mol. Cell. Probes*, 2013, **27**, 71–79.
23 X. Yang, J. Li, H. Pei, Y. Zhao, X. Zuo, C. Fan and Q. Huang, *Anal. Chem.*, 2014, **18**, 3227–3231.
24 I. Alemzadeh and S. Nejati, *J. Hazard. Mater.*, 2009, **166**, 1082–1086.
25 T. Fukuoka, H. Uyama and S. Kobayashi, *Biomacromolecules*, 2004, **5**, 977–983.
26 M. Thiyagarajan, L. A. Samuelson, J. Kumar and A. L. Cholli, *J. Am. Chem. Soc.*, 2003, **125**, 11502–11503.
27 L. A. Burzio and J. H. Waite, *Biochemistry*, 2000, **39**, 11147–11153.
28 H. D. Hill and C. A. Mirkin, *Nat. Protoc.*, 2006, **1**, 324–336.
29 F. Li, K. Li, Z. Q. Cui, Z. P. Zhang, H. P. Wei, D. Gao, J. Y. Deng and X. E. Zhang, *Small*, 2010, **6**, 2301–2308.
30 S. Deshpande, *Enzyme immunoassays: from concept to product development*, Springer, 1996.
31 J. Singer and B. E. Volcani, *J. Bacteriol.*, 1955, **69**, 303–306.
32 J. N. Broder, *Annals of Emergency Medicine*, 1987, **16**, 1188.